PCCP

Physical Chemistry Chemical Physics
rsc.li/pccp

Volume 19
Number 1
7 January 2017
Pages 1-896

ISSN 1463-9076

PAPER
H.-P. Loock et al.
Determination of the thermal, oxidative and photochemical degradation rates of scintillator liquid by fluorescence EEM spectroscopy.

ROYAL SOCIETY
OF CHEMISTRY

ROYAL SOCIETY
OF CHEMISTRY

rsc.li/pccp

Understanding the Electrochemistry of Armchair Graphene Nanoribbons Containing Nitrogen and Oxygen Functional Groups: DFT-calculations

Florentino López-Urías*, Juan L. Fajardo-Díaz, Alejandro J. Cortés-López, Cristina L. Rodríguez-Corvera, Luis E. Jiménez-Ramírez, Emilio Muñoz-Sandoval

División de Materiales Avanzados, IPICYT, Camino a la Presa San José 2055, Lomas 4a Sección, San Luis Potosí, S.L.P., 78216, México.

Abstract

The surface and edges chemistry are vital points to assess a specific application of graphene and other carbon nanomaterials. Based on first-principles density functional theory, we investigate twenty-four chemical functional groups containing oxygen and nitrogen atoms anchored to the edges of armchair graphene nanoribbons (AGNRs). Results for band structures, formation energy, band gaps, electronic charge deficit, oxidation energy, reduction energy, and global hydrophilicity index are analyzed. Among the oxygen functional groups, the carbonyl, anhydride, quinone, lactone, phenol, ethyl-ester, carboxyl, α-ester-methyl, and methoxy act as electron-withdrawing groups, conversely, pyrane, pyrone, and ethoxy act as electron-donating groups. In the case of nitrogen-functional groups, the amine, N-*p*-toluidine, ethylamine, pyridine-N-oxide, pyridone, lactam, and pyridinium transfer electrons to the AGNRs. The nitro, amide, and N-ethylamine act as electron-withdrawing groups. The carbonyl and pyridinium group-AGNR show metallic behavior. The formation energy calculations revealed that AGNRs with pyridinium, amine, pyrane, carbonyl, and phenol are the most stable structures. Global hydrophilicity index, quinone, and N-ethylamine groups showed the most significant values, suggesting they are highly efficient in accepting electrons from other chemical species. The oxidation and reduction energies as a function of the ribbon's width are discussed for AGNR with quinone, hydroquinone, nitro, and nitro+2H. Besides, we discuss the role of nitrogen-doping in AGNRs on the oxidation and reduction energies for quinone and hydroquinone functional groups.

Keywords: *Carbon, doping, nitrogen, oxygen, functionalization, modeling*

Correspondence author: flo@ipicyt.edu.mx

1. Introduction

For decades, graphite nanomaterials have attracted attention due to their broad range of applications such as absorbents,[1] catalysis,[2-3] supercapacitors,[4-6] among others. Nowadays, many experimental and theoretical works have poured efforts to understand the surface and edge chemistry of novel carbon nanomaterials such fullerenes,[7] carbon nanotubes,[8] graphene,[9] carbon nanoribbons.[10] Graphene and graphite nanoribbons are one-dimensional systems with intrinsic edges.[11] The armchair graphene nanoribbons (AGNRs) exhibit a semiconductor behavior with an interesting energy bandgap (E_{gap}) depending on the width of the ribbon, which decreases with AGNRs width. There exist three distinct families (n=3p, 3p+1, and 3p+2), where p and n are positive integers (n is the number of carbon atoms in the zigzag chains perpendicular to the periodic axis). First-principles studies have predicted that the energy gap $E_{gap}(n=3p+1) > E_{gap}(n=3p) > E_{gap}(n=3p+2)$.[12] On the other hand, functional groups are a set of atoms with their characteristics being responsible for chemical reactions carried out at the surface or edges of graphite materials.[13-16] For example, the most common oxygen functional groups are carbonyls (C=O), carboxylic acids (R-COOH), phenols (C-OH), quinone (C=O), ester (C-COO-C), ethers (C-O-C), lactone (R-COO-R'). Carbonyl, carboxyl acid, phenol, and simple amine groups are hydrophilic,[17] the ester and ether groups are hydrophobic instead.[18-19] Furthermore, carbonyl groups are crucial in many chemical reactions such as dehydrogenation process (transformation of ethylbenzene to styrene),[20] reduction of phenols, and alkanes,[2,21] and the formation of aromatic compounds using cyclic alkanes.[22] On the other hand, carboxylic acids participle actively in the formation of esters, aldehydes, and ketones.[23] The production of carboxylic acids is a result of an active oxidation process of aldehydes and continuous oxidation of hydrocarbons.[24,25] Regarding nitrogen-functional groups, these have played a crucial role in diverse applications of carbon materials.[26-30] The most common nitrogen functional groups are amine, amide, and nitrogen oxide. Amines can capture CO_2 and transfer electrons to the carbon material[31] and have also been shown great potential on the oxygen reduction reaction (ORR), enhancing the electrocatalytic activity.[32,33] In the same way, doping graphite materials with boron, phosphorus, or silicon, and heteroatoms are also an attractive topic.[34,35]

Theoretical studies of functionalized graphite materials are a very current issue to understand the surface and edges chemistry of novel carbon nanomaterials.[36,37] Qi et al.[38] reported first-principles calculations of O_2 and single O- atom placed on the basal plane of a graphite cluster. They investigated how the adsorption properties are affected for hydroxyl, carbonyl, quinone, and carboxyl groups attached at the edges of graphite clusters. Wagner et al.[39] investigated −F, −Cl, −Br, −S, −OH, −SH chemical species anchored at the edges of zigzag, armchair, and reconstructed Klein-type graphene nanoribbons.[40,41] They demonstrated that the bandgap of AGNRs depends on the variation of edge-functional groups, whereas in zigzag graphene nanoribbons (ZGNRs) and reconstructed Klein edge GNRs are mostly insensitive to the choice of edge-functional group. Recently, Radovic et al.[42] investigated the quinone/hydroquinone transition in small graphene clusters. They claimed that carbene-type zigzag carbon atoms emerge as the most likely candidates for electrochemically and electrocatalytically active sites. Li et al.[43] evaluated by DFT calculations the nucleophilicity of oxygen functional groups (carboxyl, diketone, ketone, lactone, and quinone) on the graphene. Their results suggested that the quinone group is the most nucleophilic site; however, they also found that diketone and ketone are much less active than the quinone group toward an electrophilic attack. Gracia-Espino et al.[44] investigated the transport properties into and at the edges of armchair graphene nanoribbons by considering doping (boron, nitrogen, oxygen, silicon, phosphorus, and sulfur) and functional groups (borane, amine, hydroxyl, thiol, silane, silene, phosphine, and phosphorene). Their results suggest that graphene nanoribbons could be functionalized at the inner sections keeping their transport characteristics and retaining the typical chemical reactivity of doped nanocarbons.

In this work, we investigate the effects of nitrogen- and oxygen- functional groups on the electronic properties of a semiconducting AGNR using first-principles density functional theory calculations. The systems consist of AGNRs with functional groups hosted at its edges. We study more than 24 different functional groups containing nitrogen and oxygen atoms. Usually, oxygen functional groups promote p-type doping. However, ethoxy, pyrone, and pyrane functional groups inject electrons to armchair graphene nanoribbons. Nitrogen functional groups are

excellent for improving the efficiency of lithium-ion batteries due to the charge injection promoted by these groups. Similar to oxygen functional groups, we also found some nitrogen exceptions such as amide, nitro, and N-ethylamine functionalities that pulled out electrons from the AGNRs.

2. Methodology

Spin-polarization electronic calculations were performed using density functional theory (DFT).[45,46] The generalized gradient approximation with the Perdew, Burke, and Ernzerhof parametrization was chosen for the exchange-correlation functional[47] as implemented in the SIESTA code[48]. The wave functions for the valence electrons were represented by a linear combination of pseudo-atomic numerical orbitals using a double-ζ polarized basis (DZP),[49] while the core electrons by norm-conserving Troullier-Martins pseudopotentials in the Kleinman-Bylander non-local form.[50,51] The real-space grid used for charge and potential integration is equivalent to a plane wave cut-off energy of 150 Ry. The AGNRs are periodic in the x-axis. We used a supercell containing three primitive unit cells of 13-AGNR (n=13, see figure S1) with 78 atoms. In the non-periodic axis, we used a minimum of 30 Å to avoid lateral interactions. A sampling of the 1D Brillouin zones was carried out with $20 \times 1 \times 1$ Monkhorst-Pack grids. Density matrix and energy tolerances were both taken as 10^{-5} eV. We considered the ribbon´s edge passivation with hydrogen atoms.[52] A variable cell structural relaxation was performed on all systems to include the strain effects introduced by the dopant atom or the functional groups. The geometry optimization was performed by conjugate gradient minimization until the maximum force was < 0.04 eV/Å. The formation energy (E_{form}) was determined by:

$$E_{form} = E_{pristine} - E_{funct}$$

Where E_{funct} refers to the total energy of the complex system (functional group + AGNR) and $E_{pristine}$ is the total energy of the pristine AGNR (edges passivated with hydrogen). Within the limitations of Koopmans' theorem[53] and the DFT approach, we calculate the global electrophilicity index (ω). Here ω is a measure of the capacity of

a molecule or atom to attract electrons from other chemical species. In accord with Parr et al.[54] $\omega = \mu^2 / 2\eta$, where $\mu \approx (E_v + E_c)/2$ is the chemical potential and $\eta \approx (E_v - E_c)$ is the chemical hardness. E_v and E_c refer to valence band maximum and conduction band minimum energies, respectively. We consider that the oxidation potential corresponds to the valence band maxima (VBM) energy (oxidation usually takes out an electron from the VBM energy) and the reduction energy to the conduction band minimum (CBM) energy (reduction incorporates an electron to the CBM). Hereafter, we refer to VBM and CBM energies as oxidation and reduction energies, respectively.

3. Results and discussion

Before discussing results on the functional groups, the effects of nitrogen doping AGNRs are addressed and compared to the pristine (undoped) case. We used three ways for the incorporation of the nitrogen atoms in graphite structures. The N-Quaternary doping where nitrogen atom substitutes a carbon atom, N-Pyridinic doping is generated around a vacancy, here nitrogen atoms replace low coordinated carbon atom around the vacancy, the N-Pyrrolic doping occurs when a nitrogen atom substitutes a carbon atom belonging to the pentagonal ring. Figure 1 displays the optimized structures of the pristine and N-doped AGNRs and the corresponding band structure calculation in figure 2. N-doped AGNRs exhibited bands that crossing the Fermi level (see red dashed line in figure 2) becoming metallic. When we compared with the pristine case, it is clear that the N-Quaternary doping case promoted a shift to the Fermi level toward the conduction band due to an extra pi-electron. Conversely, for N-Pyridinic and N-Pyrrolic doping, developed a change in the Fermi level toward the valence bands. Two flat bands for the N-pyridinic cases were observed just below the Fermi level (see arrow in figure 2c); the wave function associated with these bands exhibited electron localization at the doping defect (see figure S2). The interatomic distances between the nitrogen with the first carbon neighbor are 1.419, 1.352, and 1.423 Å for N-Quaternary, N-pyridinic, N-Pyrrolic, respectively. The Mulliken population analysis yielded 4.634, 4.80, and 5.030 electrons for N-Quaternary, N-pyridinic, N-Pyrrolic, respectively. Thus, the nitrogen atom lost 0.366

and 0.2 electron for N-Quaternary and N-pyridinic fashion, respectively. The metallic behavior of N-doped AGNRs disappeared with the hydrogenation of nitrogen atoms (see figure S3, Supplementary Information). This fact is due to the hydrogen atom induces a charge transfer from P_z to P_x and P_y orbitals in nitrogen atom; thus, a large amount at charge is accumulated around the nitrogen (see charge density plots in figure S4).

Figure 3 displays the optimized structures of nitrogen-functional groups attached at the edges of AGNRs (top and perspective views). We show results for amine, amine, ethylamine, N-ethylamine, pyridinium, amide, lactam, N-p-toluidine, nitro, pyridine-N-oxide, pyridone, hydrazone, and enamine. Figure 4 shows the band structure calculations for all considered functional groups. Notice that the semiconducting behavior dominates. However, the pyridinium group showed a metallic behavior, here, a band crosses the Fermi level (red dashed line). Nevertheless, the hydrogenated pyridinium group exhibited a semiconducting behavior (see figure S5, Supplementary Information). Notice also that the N-ethylamine showed a flat band just below the Fermi level. The wave functional associated with this flat band exhibited an electron localization in the functional group (see figure S6).

Table 1 shows the results of nitrogen-functional on the formation energy, charge transfer, E_v, E_c, bandgap (E_c-E_v), and ω. Mostly, the band gaps are less than the obtained for the pristine case (0.83 eV), except for the lactam case with a bandgap of 0.85 eV. The pyridinium case showed a zero band-gap. The pyridinium and amine groups were exhibited the lowest formation energies, whereas N-p-toluidine, nitro, and amide functional groups showed the highest formation energies. The electronic charge (a positive value means that the ribbons lost electronic charge, while negative values represent gained electronic charge)-yielded negative values for amine, enamine, N-p-toluidine, ethylamine, pyridine-N-oxide, pyridine, hydrazone, lactam, and pyridinium, promoting the n-type doping in the AGNRs. On the contrary, in the case of the nitro, amide, and N-ethylamine, the charge transference yield positive values.

Notice also that the values of E_v and E_c are very sensitive to the functional group attached to the edge of the AGNR. Systems with large negative values of E_v (E_c) are energetically hard (easy) to be oxidized (reduced). Therefore, from the results of table 1, hydrazone, ethylamine, and amine functionalities are easy to be oxidized, whereas the nitro and lactam groups are hard to be oxidized. Also, nitro, N-ethylamine, and pyridine-N oxide could be functionalities easy to be reduced. This fact could explain electrochemical measurements in nitrogen-doped or nitrogen-functionalized carbon graphite materials where broader anodic peaks are present.[32,55,56] Therefore, the redox peaks could be due not only to quinone-hydroquinone but also to the nitro, pyridine-N oxide, and N-ethylamine groups. Results for ω revealed that N-ethylamine and nitro groups exhibited the highest values, suggesting the capacity of these groups to capture electrons.

Figure 5 displays the optimized structures of functional groups containing oxygen (carbonyl, carboxyl, ethyl-ester, methoxy, pyrone, lactone, phenol, quinone, ethoxy, α-ester-methyl, pyrane, and anhydride) bonded at the edges of AGNRs (top and perspective views). Band structure calculations revealed how the electronic properties depended on the functional groups (figure 6). The AGNRs remained semiconducting, and only the carbonyl groups exhibited metallic features. The pyrane functional group (O-C-O) presented a non-dispersive state just below the Fermi level. The quinone group showed a quasi-non-dispersive state just above the Fermi level.

Table 2 shows the results of oxygen-functional on the formation energy, charge transfer, E_v, E_c, bandgap (E_c-E_v), and ω. The pyrane, quinone, and lactone showed the lowest bandgaps. Notice that pyrone exhibited a larger bandgap than the obtained for the pristine case (0.852 eV). The band gaps of systems containing ethyl-ester, methoxy, ethoxy, a-ester-methyl, and carboxyl are close to the value of the pristine system. The pyrane, carbonyl, and phenol cases showed the lowest formation energies. The formation energy results are qualitatively in accord with Figueiredo and coworkers.[57] They reported the delivery of CO and CO_2 with the thermal decomposition of

oxygen functional groups. They found that carbonyls, quinones, and lactones are the most thermally stable, followed by phenols and carboxylic acids.

Regarding the charge transfer, the carbonyl, anhydride, and quinone groups exhibited the most significant positive charge deficit in the oxygen atom, leading to p-type doping in the AGNRs. In the case of the ethoxy, pyrone, and pyrane groups, they provide electrons to the ribbons, leading to n-type doping. From values of E_v and E_c (table 2), the phenol, pyrane, alpha-ester-methyl, methoxy, ethyl-ester, ethoxy are energetically favorable to be oxidized whereas quinone and anhydride are energetically favorable to be reduced. The quinone showed the highest value of the hydrophilicity index, followed by pyrane, anhydride, and lactone functional groups.

Oxidation energies of nitrogen and oxygen functionalities are given in figure 7a. Interestingly, all oxygen functional groups are enclosed between the quinone and hydroquinone, which are hard and easy to oxidize, respectively. Band-structure and optimized structure of the hydroquinone groups can be seen in figure S7. The hydroquinone showed the highest oxidation energy within the oxygen-functional groups. On the contrary, the quinone can be straightforward to reduce (see figure 7d). The ethoxy, ethyl-ester, methoxy, pristine, phenol, and pyrane showed low oxidation energies, very competitive with the hydroquinone group. The nitrogen-functional also displayed exciting trends. The N-Quaternary-H groups showed the lowest oxidation energy, less than that observed for the hydroquinone. We found that hydrazone, ethylamine, N-pyrrolic-H, amine, N-ethylamine, and N-*p*-toluidine exhibited low oxidation energy. On the other hand, the nitro, lactam, pyridinic-N oxide, pyridine-N, pyridone, and amide are groups hard to oxidize.

Now, we discuss the effect of nitrogen-doping (N-Quaternary-H) on oxidation and reduction energies of hydroquinone and quinone respective (). Here, the nitrogen doping was placed in different positions across the ribbon, figure 7b. Label A refers to pristine (undoped) hydroquinone and quinone, whereas labels B-G correspond

to hydroquinone and quinone with N-doping. Label B (G) displays the structure with nitrogen atom closest (farthest) to the edge. The difference of energies between the quinone and hydroquinone can give insight into the separation voltage between the peaks in a redox process. The systems showed significant changes in the oxidation and reduction energies in comparison with the pristine cases. Both oxidation and reduction energies were sensitive to the nitrogen position. For nitrogen closes to the edge (label B), the oxidation and reduction energy occur in almost similar energies. For label D, the nitrogen position yielded a light increment of the reduction energy of the quinone group when compared with the pristine quinone. Usually, in cyclic voltammetry, the oxidation peak appears on the right side of the reduction peak, this situation corresponds to pristine case and N-doped AGNRs with labels C and F. Conversely, for N-doped AGNRs corresponding to labels B, D, E, and, G, the oxidation peak should appear on the left side of the reduction peak. The nitrogen positions in figure 7b can also be seen as nitrogen-doping sublattice-1 (B, D, and F) and sublattice-2 (C, E, and G). Therefore, the oxidation and reduction energies could provide information that could give insights on what sublattice is doping.[58,59]

Ribbon width dependent reduction and oxidation energies revealed interesting trends (figure 8). Results for the quinone and hydroquinone are shown in figure 8a. The quinone is energetically more favorable to reduce (high negative energy required for trapping an electron) for ribbons family $n=3p$ ($n=6, 9, 12, 15$) whereas the hydroquinone is energetically more favorable to oxidize (less energy required to remove an electron) for ribbons family $n=3p+2$ ($n=5, 8, 11, 14$). Ribbon family $n=3p+2$ are energetically more favorable to reduce in the nitro group, also ribbon family $n=3p+2$ are more favorable to oxidize (figure 8b). The difference between E_v and E_c is shown in figure 9. In both cases, quinone and nitro groups exhibited negative and positive values of E_v-E_c. AGNRs with $n=3p+1$ always yielded negative values, whereas AGNRs with $n=3p+2$ yielded positive values, except $n=5$.

4. Conclusions

We investigated the electronic properties of AGNRs with oxygen and nitrogen functional groups attached to its edges in the framework of first-principles density functional theory. The electronic bandgap was sensitive to the assigned functional group. The pyridinium and carbonyl case displayed a metallic behavior with bands crossing the Fermi level. Predominantly, the functional groups showed a smaller bandgap than the pristine case. The lactam and pyrone functional groups were the most energetically stable structure, whereas N-*p*-toluidine and ethoxy functional groups were the less energetically stable structures. Oxygen-functional groups pulled out electrons from the ribbon structure, promoting the p-type doping. The carbonyl group showed the most significant charge transfer, followed by the anhydride and quinone. The methoxy group showed the lowest charge transfer. Conversely, the ethoxy, pyrone, and pyrane favored n-type doping. Regarding nitrogen functional groups, these injected electrons to the ribbons favoring the n-type doping. The amine showed the lowest electron transfer, whereas the pyridinium and lactam displayed the most significant electron transfer. We found that nitro, amide, and N-ethylamine pulled out electrons from the ribbons, promoting the p-type doping.

For organic chemistry, the carbonyl group, quinone, and phenolic groups play an essential role in the redox process. Our results demonstrated that these groups are energetically stable and competitive with other functional groups. Furthermore, these showed the most significant charge transfer among the oxygen functional groups considered, which could increase the anodic and cathodic currents in electrochemical measurements. Global hydrophilicity index calculations revealed that the quinone in conjunction with pyrane, anhydride, pyrone, N-ethylamine, nitro, and pyridine N-oxide groups are efficient to exchange electrons, suggesting the participation of these groups in a redox process. Nitrogen functional groups act as electron-donating, creating a net negative charge on adjacent carbon atoms; these carbon atoms can attract cations from the cathode and act as active sites for ORR.[60] Our results demonstrated that the hydroquinone is energetically more favorable to oxidize in AGNRs with n=3p+2, while the quinone is energetically more favorable to reduce for AGNRs with n=3p. We also found that the nitrogen-doping in AGNRs modifies the oxidation and reduction energies of hydroquinone and quinone,

respectively. Our DFT results provide interesting trends that could be better quantified, including first-principles many-electron Green's function approach in the framework of GW approximation.[61] Also, for a quantitative study of redox processes, one should take into account several aspects such as the solvent, bandgap correction, work function, among others.

Author contributions

FLU and EMS designed the research and wrote the manuscript. The authors JLFD, AJCL, CLRC, and LEJR participated in the discussion of results.

Competing financial interests

The authors declare no competing financial interests.

Acknowledgments

References

1. Gracia-Espino E, López-Urías F, Terrones H, Terrones M. Novel Nanocarbons for Adsorption. In Novel Carbon Adsorbents. 1st Edition. Oxford, UK: Elsevier Inc. 2012. p. 3-34.

2. S. Navalon, A. Dhakshinamoorthy, M. Alvaro, M. Antonietti, H. Garcia. Active sites on graphene-based materials as metal-free catalysts. *Chem. Soc. Rev., 2017,* **46**, 4501.

3. Y. Li, Y. Zhao, H. Cheng, Y. Hu, G. Shi, L. Dai, L. Qu. Nitrogen-Doped Graphene Quantum Dots with Oxygen-Rich Functional Groups. *J. Am. Chem. Soc.,* 2012, **134**, 15.

4. D. Hulicova-Jurcakova, M. Seredych, G. Qing Lu, T. J. Bandosz. Combined Effect of Nitrogen- and Oxygen-Containing Functional Groups of Microporous Activated Carbon on its Electrochemical Performance in Supercapacitors. *Adv. Funct. Mater.,* 2009*, ***19**, 438.

5. H. R. Byon, B. M. Gallant, S. Woo Lee, Y. Shao-Horn. Role of Oxygen Functional Groups in Carbon Nanotube/Graphene Freestanding Electrodes for High Performance Lithium Batteries. *Adv. Funct. Mater.,* 2013*, ***23**, 1037.

6. S. W. Lee, N. Yabuuchi, B. M. Gallant, S. Chen, Byeong-Su Kim, P. T. Hammond, et al. High-power lithium batteries from functionalized carbon-nanotube electrodes. *Nat. Nanotechnol.,* 2010*, ***5**, 531.

7. H. W. Kroto, A. W. Allaf, S. P. Balm. C_{60}-Buckminsterfullerene. *Chem. Rev.,* 1991*, ***91**, 1213.

8. S. Iijima, T. Ichihashi. Single-shell carbon nanotubes of 1-nm diameter. *Nature,* 1993, **363**, 603.

9. A. K. Geim, K. S. Novoselov. The rise of graphene. *Nat. Mater., 2007,* **6**, 183.

10. M. Fujita, K. Wakabayashi, K. Nakada, K. Kusakabe. Peculiar Localized State at Zigzag Graphite Edge. *J. Phys. Soc. Jpn.,* 1996*, ***65**, 1920.

11. Gracia-Espino E, López-Urías F, Kim YA, Hayashi T, Muramatsu H, Terrones H, et al. Novel Carbon-Based Nanomaterials: Graphene and Graphitic Nanoribbons. In Handbook of Advanced Ceramics: Materials, Applications, Processing, and Properties: Second Edition. Elsevier Inc. 2013. p. 61-87.

12. Son, Y.W.; Cohen, M.; Louie S. Energy Gaps in Graphene Nanoribbons. *Phys. Rev. Lett.,* 2006*, ***97**, 216803.

13. A. Eftekhari, H. Garcia. The necessity of structural irregularities of the chemical applications of graphene, *Mater. Today Chem.,* 2017, **4**, 1.

14. L. R. Radovic, Bradley Boc. What (exactly) is on the edges of graphene layers in carbon: The unfolding story. *Fuel Chemistry Division,* 2002, **47**(2), 428.

15. H. P. Boehm. Surface Properties of Carbons. *Stud. Surf. Sci. Catal.,* 1989*, ***48**, 145.

16. Y. Byun, M. Cho, D. Kim, Y. Jung, A. Coskun. Edge-Functionalized Graphene Nanoribbon Frameworks for the Capture and Separation of Greenhouse Gases. *Macromolecules,* 2017, **50**, 523.

17. S. Kundo, Y.Wang, W. Xia, M. Muhler. Thermal stability and reducibility of oxygen-containing functional groups on multiwalled carbon nanotube surfaces: A quantitative high-resolution XPS and TPD/TPR Study. *J. Phys. Chem.,* 2008, **112**, 16869.

18. F.M. Menger, M.E. Chlebowski. Is the ether group hydrophilic or hydrophobic?. *Langmuir*, 2005, **21** (7), 2689.

19. T. Shikata, M. Okuzono. Are all polar molecules hydrophilic? Hydration numbers on ketones and esters in aqueous solutions. *J. Phys. Chem. B,* 2013, **117** (25), 7718.

20. W. Qi, W. Liu, B. Zhang, X. Gu, X. Guo, D. Su. Oxidative dehydrogenation on nanocarbon: identification and quantification of active sites by chemical titration. *Angew. Chem. Int. Ed.,* 2013, **52**, 14224.

21. C. Moreno-Castilla, F. López-Ramón, F. Carrasco-Marín. Changes in surface chemistry of activated carbons by wet oxidation, *Carbon,* 2000, **38** (14), 1995.

22. L.M. Ombaka, P. Ndungu, V.O. Nyamori. Usage of carbon nanotubes as platinum and nickel catalyst support in dehydrogenation reactions. *Catal. Today,* 2013, **217**, 65.

23. F.A. Abuilaiwi, T. Laoui, M. Al-Harthi, M.A. Atieh. Modification and functionalization of multiwalled carbon nanotube (MWCNT) via Fischer esterification. *AJSE, 2010,* **35** (1C), 37.

24. P.V. Lakshminarayanan, H. Toghiani, C.U. Pittman-Jr. Nitric acid oxidation of vapor grown carbon nanofibers. *Carbon,* 2004, **42**, 2433.

25. K.A. Wepasnik, B.A. Smith, K.E. Schrote, H.K. Wilson, S.R. Diegelmann, D.H. Fairbrother. Surface and structural characterization of multi-walled carbon nanotubes following different oxidative treatments. *Carbon,* 2011, **49** (1), 24.

26. W. Shin, H. M. Jeong, B.G. Kim, J.K. Kang, J.W. Choi. Nitrogen-doped multiwall carbon nanotubes for lithium storage with extremely high capacity. *Nano Lett.,* 2012, **12** (5), 2283.

27. Y. Liu, X. Wang, Y. Dong, Z. Wang, Z. Zhao, J. Qiu. Nitrogen-doped graphene nanoribbons for high-performance lithium ion batteries. *J. Mater. Chem. A, 2014,* **2**, 16832.

28. Y. Qian, L. Jiang, Z. Ullah, Z. Guan, C. Yu, S. Zhu, et al. Enhanced lithium storage performance of graphene nanoribbons doped with high content of nitrogen atoms. *Nanotech.,* 2019, **30**, 225401.

29. U. Rajaji, R. Arumugam, S. Chen, T. Chen, T. Tseng, S. Chinnapaiyan, et al. Graphene Nanoribbons in Electrochemical Sensors and Biosensors: A Review. *Int. J. Electrochem. Sci.,* 2018*,* **13**, 6643.

30. M. M. Pour, A. Lashkov, A. Radocea, X. Liu, T. Sun, A. Lipatov , et al. Laterally extended atomically precise graphene nanoribbons with improved electrical conductivity for efficient gas sensing. *Nat. Commun.,* 2017, **8**, 1.

31. G. Qi, L. Fu, E.P. Giannelis. Sponges with covalent tethered amines for high-efficiency carbon capture. *Nat. Commun.,* 2014, **5**, 1.

32. C. Zhang, R. Hao, H. Liao, Y. Hou. Synthesis of amino-functionalized graphene as metal-free catalyst and exploration of the roles of various nitrogen states in oxygen reduction reaction. *Nano Energy,* 2013, **2**(1), 88.

33. C. K. Chua, Z. Sofer, J. Luxa, and M. Pumera. Selective Nitrogen Functionalization of Graphene by Bucherer-Type Reaction. *Chem. Eur. J.,* 2015*,* **21**, 8090.

34. S. Kawai, S. Nakatsuka, T. Hatakeyama, R. Pawlak, T. Meier, J. Tracey, et al. Multiple heteroatom substitution to graphene nanoribbon. *Sci. Adv.,* 2018, **4**, 7181.

35. M. Wang, W. Wang, T. Qian, S. Liu, Y. Li, Z. Hou, et al. Oxidizing Vacancies in Nitrogen-Doped Carbon Enhance Air-Cathode Activity. *Adv. Mater.,* 2019, **31**, 1803339.

36. B. Genorio, A. Znidarsic. Functionalization of graphene nanoribbons. *J. Phys. D: Appl. Phys.,* 2014, **47**, 094012.

37. J. Park, M. Yan. Covalent Functionalization of Graphene with Reactive Intermediates. *Acc. Chem. Res.,* 2013*,* **46**(1), 181.

38. X. Qi, W. Song, J. Shi. Density functional theory study the effects of oxygen-containing functional groups on oxygen molecules and oxygen atoms adsorbed on carbonaceous materials. *PLOS ONE,* 2017, **12**(3), e0173864.

39. P. Wagner, C. P. Ewels, J. -J. Adjizian, L. Magaud, P. Pochet, S. Roche, et al. Band Gap Engineering via Edge-Functionalization of Graphene Nanoribbons. *J. Phys. Chem. C,* 2013, **117**(50), 26790.

40. K. Suenaga, M. Koshino. Atom-by-atom spectroscopy at graphene edge. *Nature,* 2010, **468**, 1088.

41. D. Klein. Graphitic polymer strips with edge states. *Chem. Phys. Lett.,* 1994, **217**(3), 261.

42. L. R. Radovic, A. J. A. Salgado-Casanova. Hydrogen transfer and quinone/hydroquinone transitions in graphene-based materials. *Carbon*, 2018, **126**, 443.

43. B. Li, D. Su. The Nucleophilicity of the Oxygen Functional Groups on Carbon Materials: A DFT Analysis. *Chem. Eur. J.,* 2014, **20**, 7890.

44. E. Gracia-Espino, F. López-Urías, H. Terrones, and M. Terrones. Electron Transport Study on Functionalized Armchair Graphene Nanoribbons: DFT Calculations. *RSC-Advances,* 2016, **6**, 21954.

45. P. Hohenberg, W. Kohn. Inhomogeneous electron gas. *Phys. Rev.*, 1964, **136**, B864.

46. W. Kohn, L.J. Sham. Self-consistent equations including exchange and correlation effects. *Phys. Rev.*, 1965, **140**, A1133.

47. J. P. Perdew, A. Ruzsinszky, G. I. Csonka, O. A. Vydrov, G. E. Scuseria, L.A. Constantin, et al. Restoring the density-gradient expansion for exchange in solids and surfaces. *Phys. Rev. Lett.*, 2008, **100**, 136406.

48. J. M. Soler, E. Artacho, J. D. Gale, A. García, J. Junquera, P. Ordejón, et al. The SIESTA method for ab initio order-N materials simulation. J. Phys. Condens. Matter., 2002, **14**, 2745.

49. J. Junquera, O. Paz, D. Sánchez-Portal, E. Artacho. Numerical atomic orbitals for linear-scaling calculations. *Phys. Rev. B*, 2001, **64**, 235111.

50. N. Troullier, J. L. Martins. Efficient pseudopotentials for plane-wave calculations. *Phys. Rev. B,* 1991, **43**, 1991.

51. L. Kleinman, D. M. Bylander. Efficacious form for model pseudopotentials. *Phys. Rev. Lett.,* 1982, **48**, 1425.

52. V. Barone, O. Hod, G. E. Scuseria. Electronic Structure and Stability of Semiconducting Graphene Nanoribbons. *Nano Lett.,* 2006, **6**(12), 2748.

53. T. Koopmans. Ordering of wave functions and eigenenergies to the individual electrons of an atom. *Physica* 1, 1933, 104.

54. R.G. Parr, L.v. Szentpály, S. Liu. Electrophilicity Index. *J. Am. Chem. Soc.,* 1999, **12**(9), 1922.

55. A.B. Soliman, H.S. Abdel-Samad, S.S. Abdel-Rehim, H.H. Hassan. Surface functionality and electrochemical investigations of a graphitic electrode as a candidate for alkaline energy conversion and storage devices. *Sci. Rep.,* 2016, **6**, 1.

56. I.M. Rocha, O.S.G. Soares, D.M. Fernandez, C. Freire, J.L. Figueiredo, M. F. R. Pereira. N-doped carbon nanotubes for the oxygen reduction reaction in alkaline médium: Synergistic relationship between pyridinic and quaternary nitrogen. *ChemistrySelect,* 2016, **1**(10), 2522.

57. J. L. Figueiredo, M. F. R. Pereira. The role of surface chemistry in catalysis with carbons. *Catal. Today,* 2010, **150**(1-2), 2.

58. L. Zhao et al. Visualizing Individual Nitrogen Dopants in Monolayer Graphene. *Science,* 2011, **333**(6045), 999.

59. A. Zabet-Khosousi, L. Zhao, L. Palová, M. S. Hybertsen, D. R. Reichman, A. N. Pasupathy, et al. Segregation of Sublattice Domains in Nitrogen-Doped Graphene. *J. Am. Chem. Soc.,* 2014, **136**(4), 1391.

60. X. Chen, X.-R. Chen, T.-Z. Hou, B.-Q. Li. X.-B. Cheng, R. Zhang, Q. Zhang. Lithiophilicity chemistry of heteroatom-doped carbon to guide uniform lithium nucleation in lithium metal anodes. *Sci. Adv.,* 2019, **5** (2), eaau7728.

61. L. Yang, C.-H. Park, Y.-W. Son, M. L. Cohen, S. G. Louie. Quasiparticle Energies and Band Gaps of Graphene Nanoribbons. *Phys. Rev. Lett.,* 2007*, **99**, 186801.

Physical Chemistry Chemical Physics

Tables and captions

Table 1: F. López-Urías et al.

System	E_{form}	Q	E_v	E_c	E_c-E_v	ω
N-ethylamine	6.518	0.026	-4.363	-3.834	0.530	15.875
N-p-toluidine	13.963	-0.110	-4.369	-3.596	0.773	10.255
Nitro	12.446	0.078	-4.743	-3.976	0.764	12.392
Pyridine-N-oxide	6.053	-0.118	-4.605	-3.867	0.739	12.161
Amide	9.449	0.030	-4.520	-3.733	0.788	10.815
Lactam	6.077	-0.194	-4.645	-3.786	0.858	10.348
Pyridone	6.074	-0,128	-4.533	-3.706	0.813	10.261
Amine	3.115	-0.020	-4.335	-3.563	0.772	10.099
Ethylamine	6.315	-0.112	-4.288	-3.491	0.801	9.497
hydrazone	6.086	-0.134	-4.278	-3.490	0.788	9.571
enamine	9.559	-0.032	-4.551	-3.738	0.812	10.567
Pyridinium	1.280	-0.324	-----	------	0.000	------
Pristine	0.000	--------	-4.478	-3.648	0.829	9.949

Table 1: Results for E_{form} (eV), electronic charge transfer (¯e), E_v (eV), E_c (eV), electronic bandgap (E_c-E_v), and global hydrophilicity index (ω) of AGNRs with nitrogen-functional groups. The formation energies were referenced to the formation energy of pristine AGNR. Positive values of Q mean that the AGNRs lost electrons (p-type doping), conversely, negative values indicate that the AGNRs gain electrons (n-type doping). Large values ω indicate a high capacity to capture electrons. The quinone and pyrane functional groups showed the highest values of ω.

**Table 2:** F. López-Urías et al.

| System	E_{form}	Q	E_v	E_c	E_c-E_v	ω
Quinone	9.559	0.106	-4.904	-4.289	0.636	17.184
Pyrane	2.921	-0.106	-4.506	-3.947	0.567	15.981
pyrone	7.940	-0.052	-4.758	-3.909	0.852	11.060
Phenol	4.909	0.082	-4.479	-3.698	0.783	10.711
Carboxyl	11.273	0.078	-4.558	-3.745	0.815	10.590
α-ester-methyl	12.866	0.056	-4.520	-3.711	0.815	10.468
Methoxy	6.735	0.016	-4.467	-3.661	0.800	10.251
Ethyl-ester	12.867	0.082	-4.460	-3.649	0.812	10.127
Ethoxy	8.458	-0.008	-4.443	-3.634	0.813	10.082
Lactone	11.153	0.082	-4.683	-3.968	0.715	13.081
Anhydride	17.386	0.134	-4.822	-4.057	0.736	13.472
carbonyl	4.775	0.136	---------	---------	0.000	--------
Pristine	0.000	---------	-4.478	-3.648	0.829	9.949

Table 2: Results for E_{form} (eV), electronic charge transfer ($^-$e), E_v (eV), E_c (eV), electronic bandgap (E_c-E_v), and global hydrophilicity index (ω) of AGNRs with oxygen-functional groups. The formation energies were referenced to the formation energy of pristine AGNR. Positive values of Q mean that the AGNRs lost electrons (p-type doping), conversely, negative values indicate that the AGNRs gain electrons (n-type doping). Large values ω indicate a high capacity to capture electrons. The quinone and pyrane functional groups showed the highest values of ω.

Figures and captions

Figure 1: F. López-Urías et al.
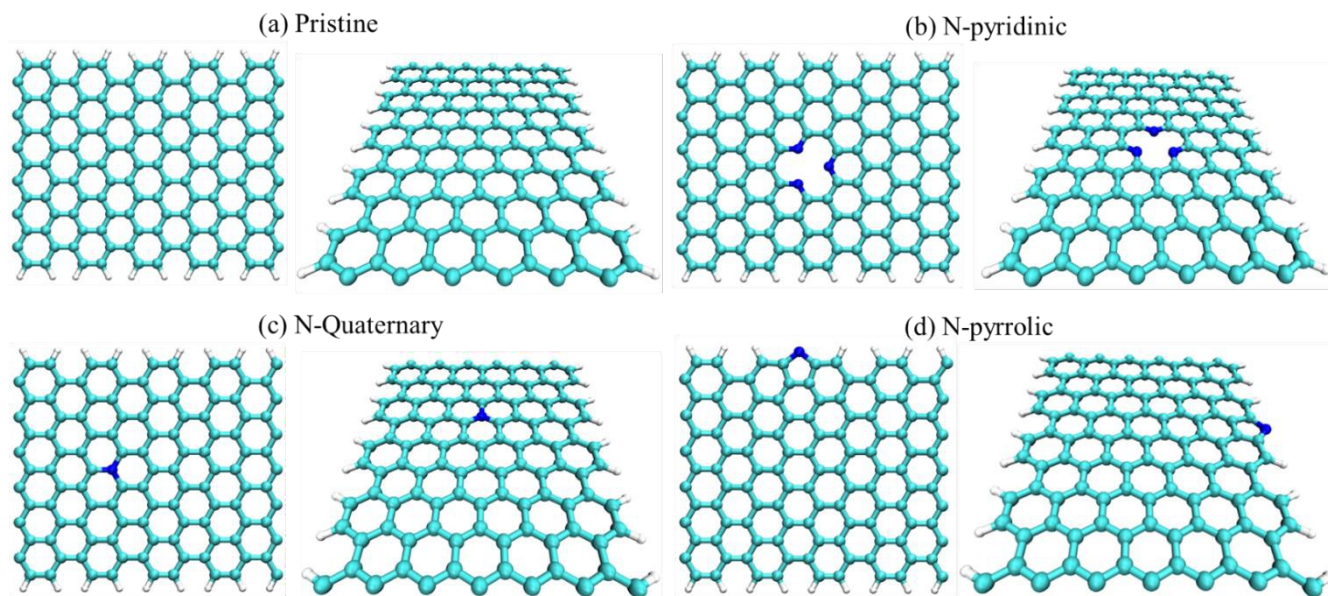
Figure 1: Ball-stick models of the optimized structures for pristine and nitrogen-doped AGNRs (top and perspective views). The edges of ribbons show hydrogen passivation. The hydrogen, carbon, and nitrogen are set in color gray, green, and blue, respectively. **(a)** Pristine, **(b)** N-pyridinic doping, **(c)** N-Quaternary doping, and **(d)** N-pyrrolic doping.
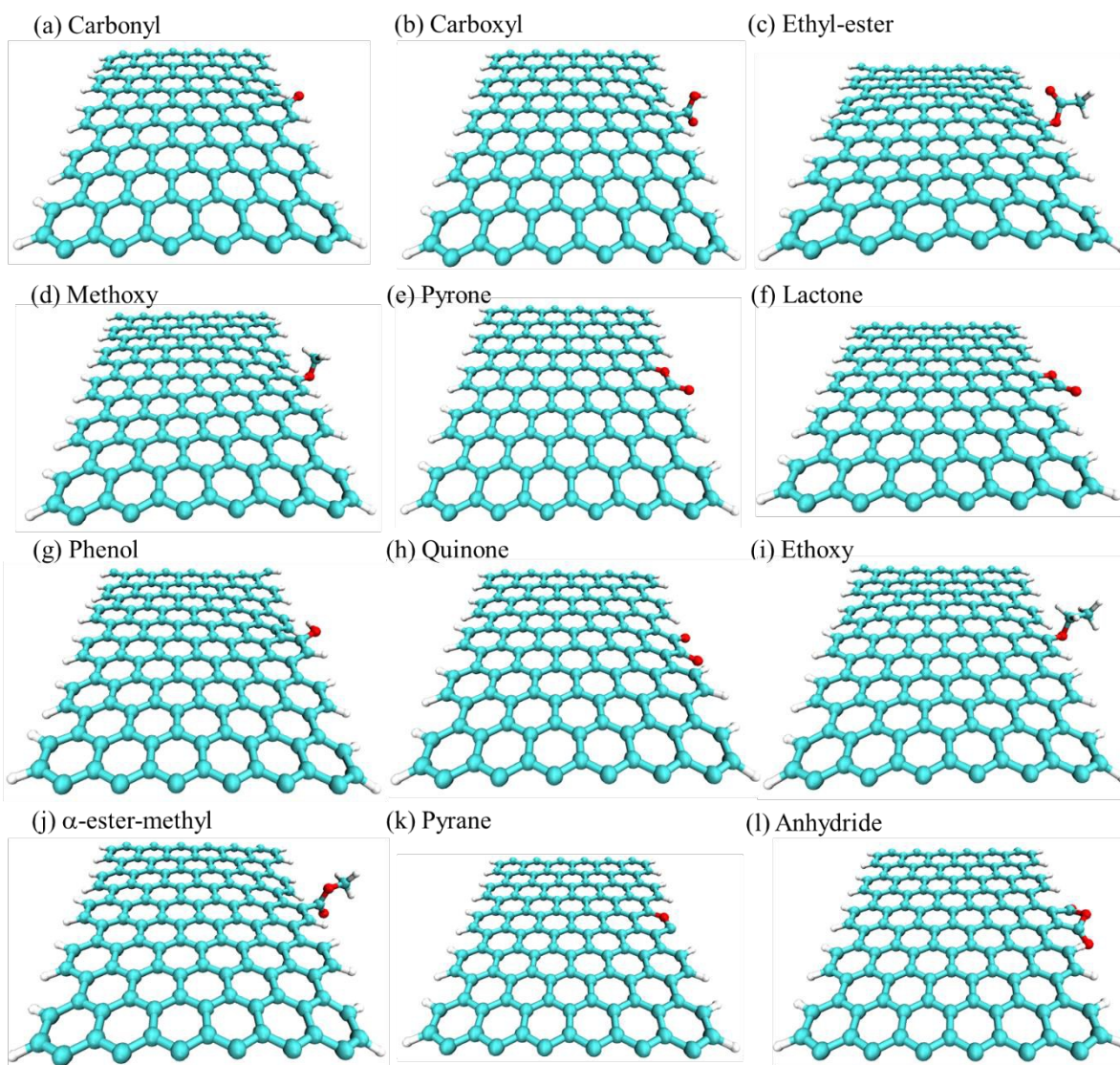
Figure 2: F. López-Urías et al.
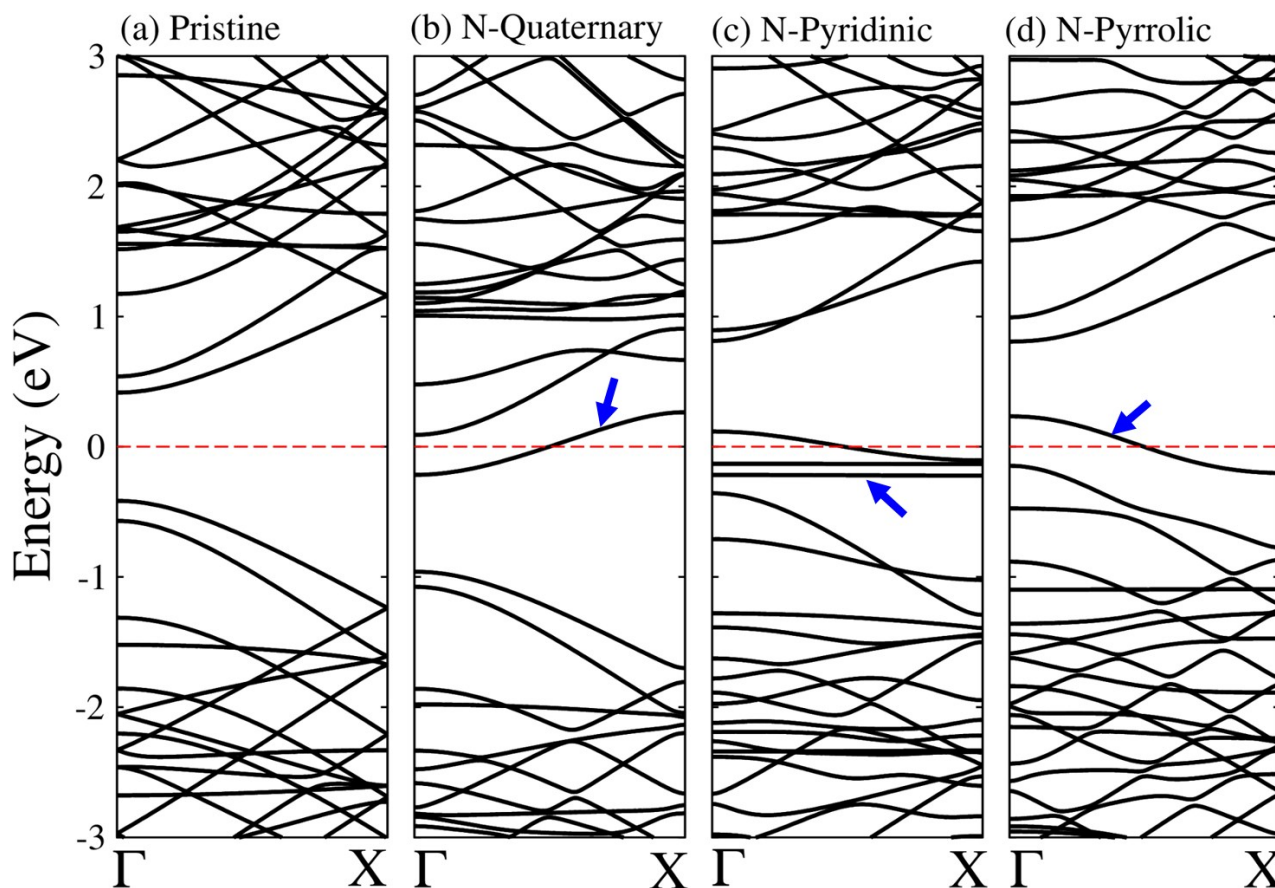
Figure 2: Band structure of pristine and nitrogen-doped AGNRs. Results for **(a)** Pristine AGNR, **(b)** N-Quaternary, **(c)** N-pyridinic, and **(d)** N-pyrrolic. In all cases, the Fermi level is zero energy (dashed line). All doping cases exhibited bands that crossing the Fermi level (metallic behavior).

Figure 3: F. López-Urías et al.
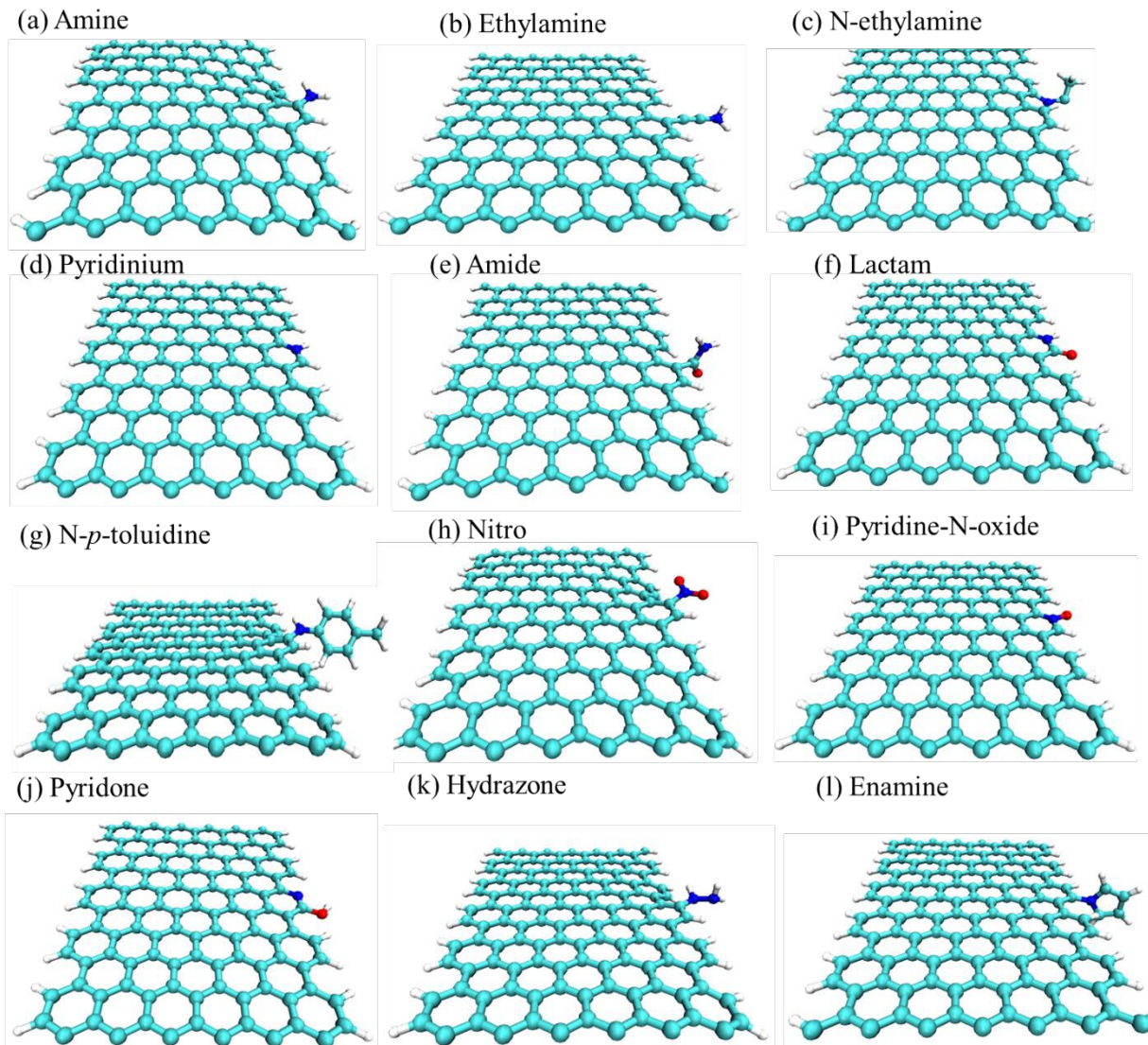
Figure 3: Ball-stick model of the optimized structures of nitrogen-functional groups attached at the edges of AGNRs (Top and perspective views). The hydrogen, carbon, nitrogen, and oxygen are set in color gray, green, blue, and red, respectively. Results for **(a)** amine, **(b)** ethylamine, **(c)** N-ethylamine, **(d)** pyridinium, **(e)** amide, **(f)** lactam, **(g)** N-*p*-toluidine, **(h)** nitro, **(i)** pyridine N-oxide, **(j)** pyridone, **(k)** hydrazone, and **(l)** Enamine.

21

Figure 4: F. López-Urías et al.
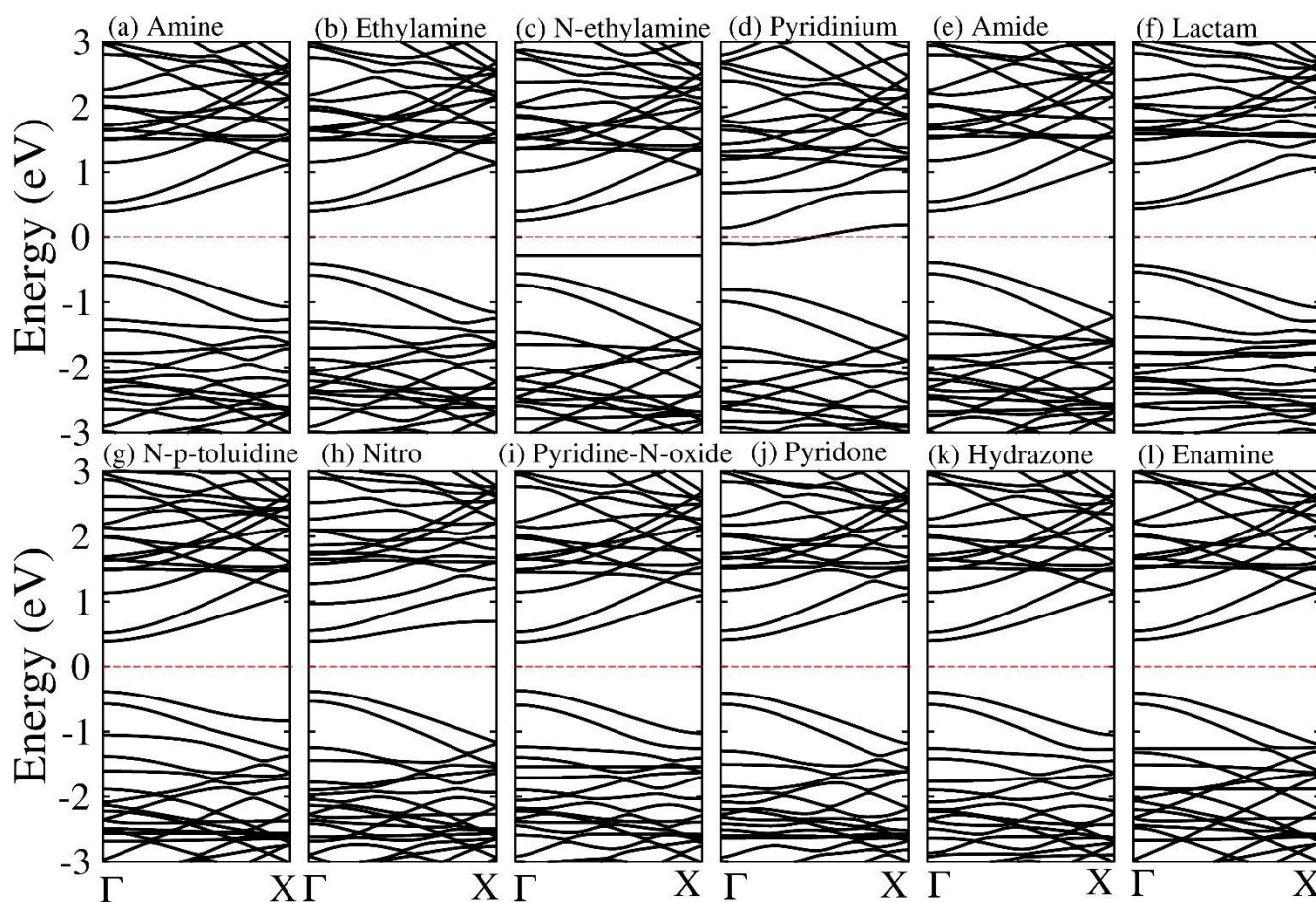
Figure 4: Band structure calculations of nitrogen-functionalized AGNRs. In all cases, the Fermi level is in zero energy (dashed line). Results for **(a)** Amine, **(b)** ethylamine, **(c)** N-ethylamine, **(d)** pyridinium, **(e)** amide, **(f)** lactam, **(g)** N-*p*-toluidine, **(h)** nitro, **(i)** pyridine N-oxide, **(j)** pyridone, **(k)** hydrazone, and **(l)** enamine. The corresponding optimized structures can be seen in figure 3.

Figure 5: F. López-Urías et al.

(a) Carbonyl (b) Carboxyl (c) Ethyl-ester

(d) Methoxy (e) Pyrone (f) Lactone

(g) Phenol (h) Quinone (i) Ethoxy

(j) α-ester-methyl (k) Pyrane (l) Anhydride

Figure 5: Ball-stick model of the optimized structures of oxygen-functional groups attached at the edges of AGNRs (Top and perspective views). Results for **(a)** Carbonyl, **(b)** carboxyl, **(c)** ethyl-ester, **(d)** methoxy, **(e)** pyrone, **(f)** lactone, **(g)** phenol, **(h)** quinone, **(i)** ethoxy, **(j)** α-ester-methyl, **(k)** pyrane, and **(l)** anhydride.

Figure 6: F. López-Urías et al.
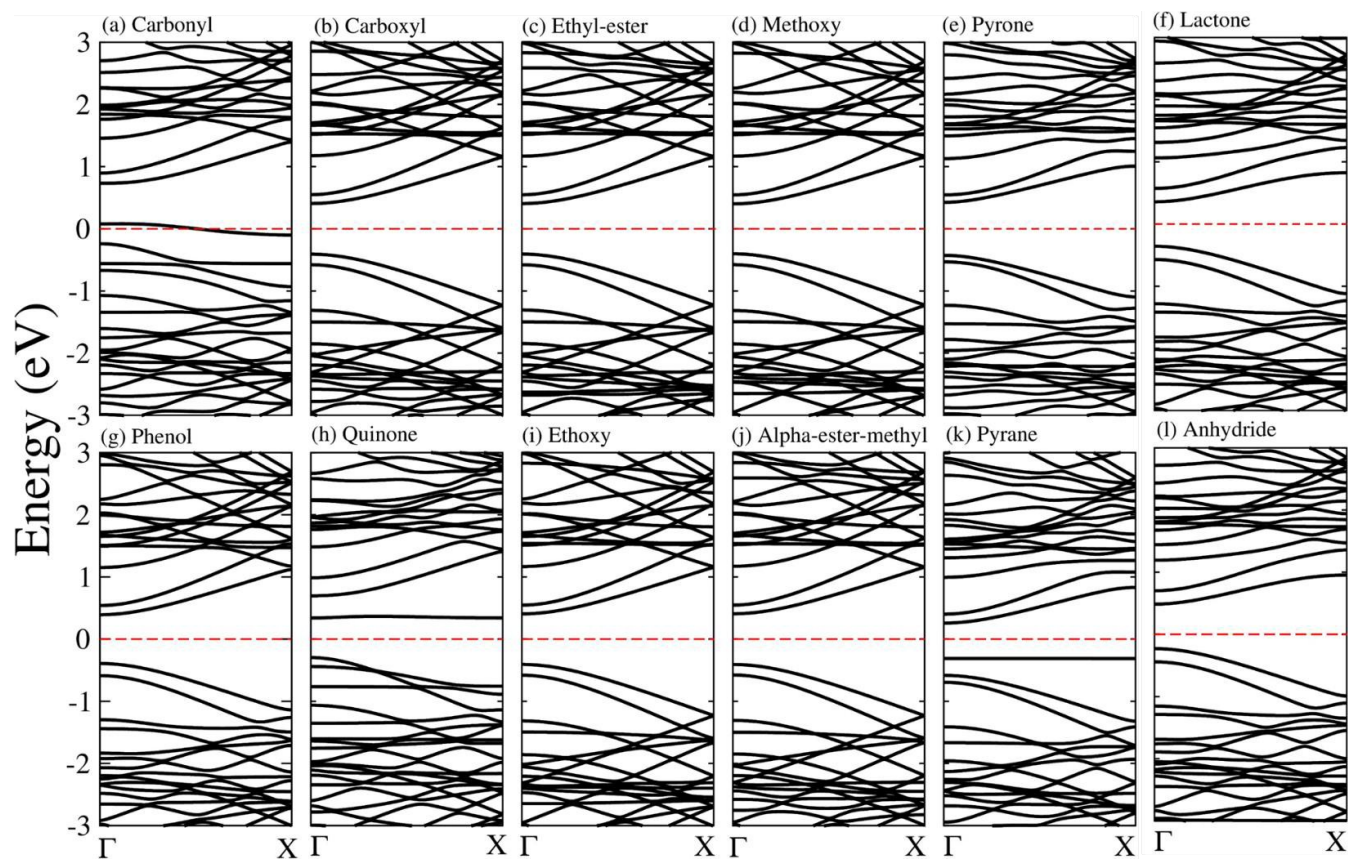
Figure 6: Band structure of oxygen-functionalized AGNRs. In all cases, the Fermi level is in zero energy (dashed line). Results for **(a)** Carbonyl, **(b)** carboxyl, **(c)** ethyl-ester, **(d)** methoxy, **(e)** pyrone, **(f)** lactone, **(g)** phenol, **(h)** quinone, **(i)** ethoxy, **(j)** α-ester-methyl, **(k)** pyrane, and **(l)** anhydride. The corresponding optimized structures can be seen in figure 5.

Figure 7: F. López-Urías et al.
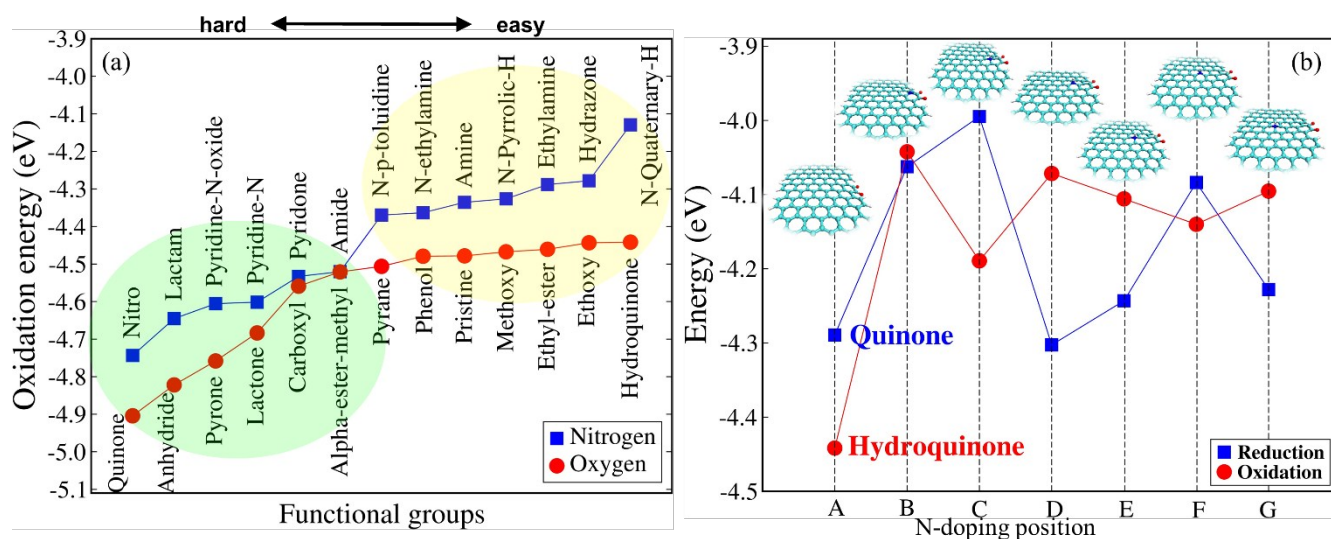
Figure 7: (a) Oxidation energy for nitrogen and oxygen functional groups attached at the edge of an AGNR. The oxidation energies close to that of the hydroquinone groups could help unmask several signals in cyclic voltammetry of nitrogen-doped and N-functionalized graphite materials.[32] **(b)** Reduction energies for the quinone and oxidation energies for hydroquinone in pristine and nitrogen-doped AGNRs. Label A displays results for the pristine quinone and hydroquinone. Labels B, C, D, E, F, and G refer to the different position of the nitrogen atom. For each label, the optimized structures of quinone groups are displayed. The corresponding structures of hydroquinone groups exhibit hydrogenated oxygen atoms (not shown).

Figure 8: F. López-Urías et al.
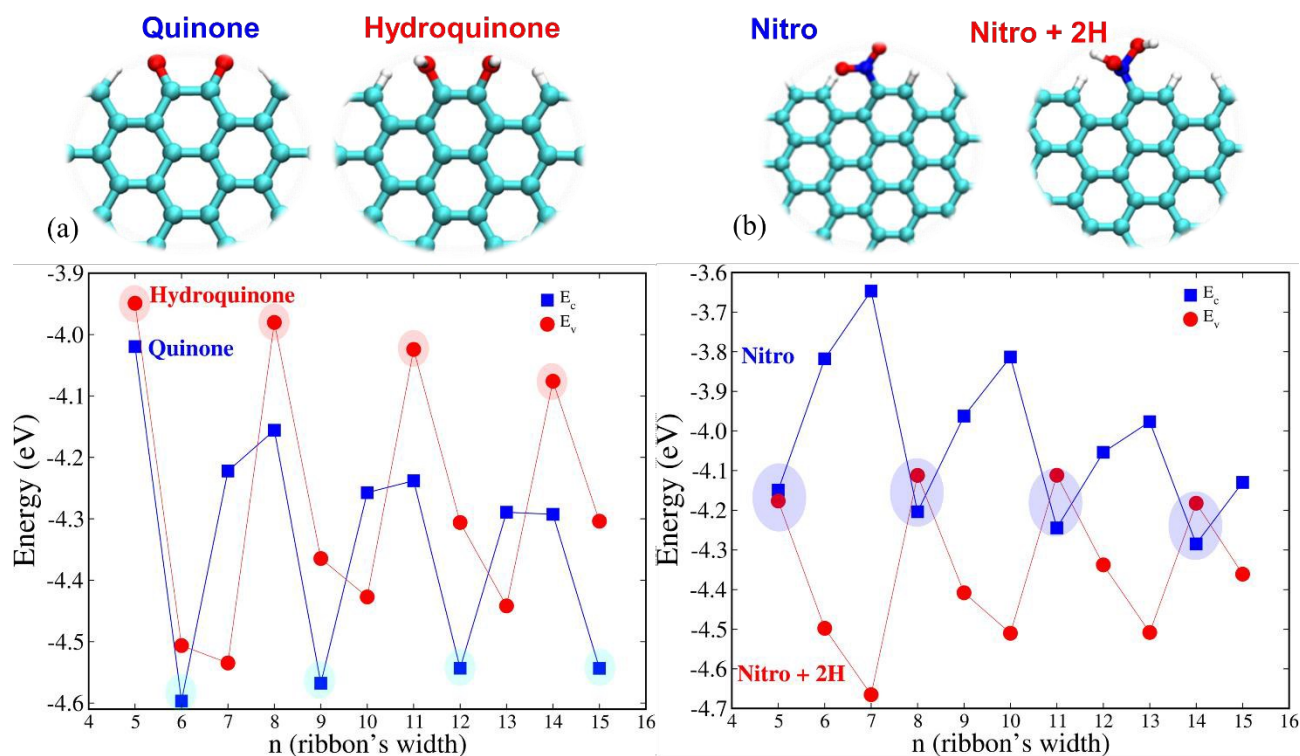
Figure 8: oxidation and reduction energies (E_v and E_c) as a function of n (ribbon's width), where n refers to the number of dimers across the ribbon width (see figure S1). Reduction energies for quinone and nitro groups and oxidation energies for hydroquinone and nitro+2H. The ball-stick models are shown on the top.

Figure 9: F. López-Urías et al.
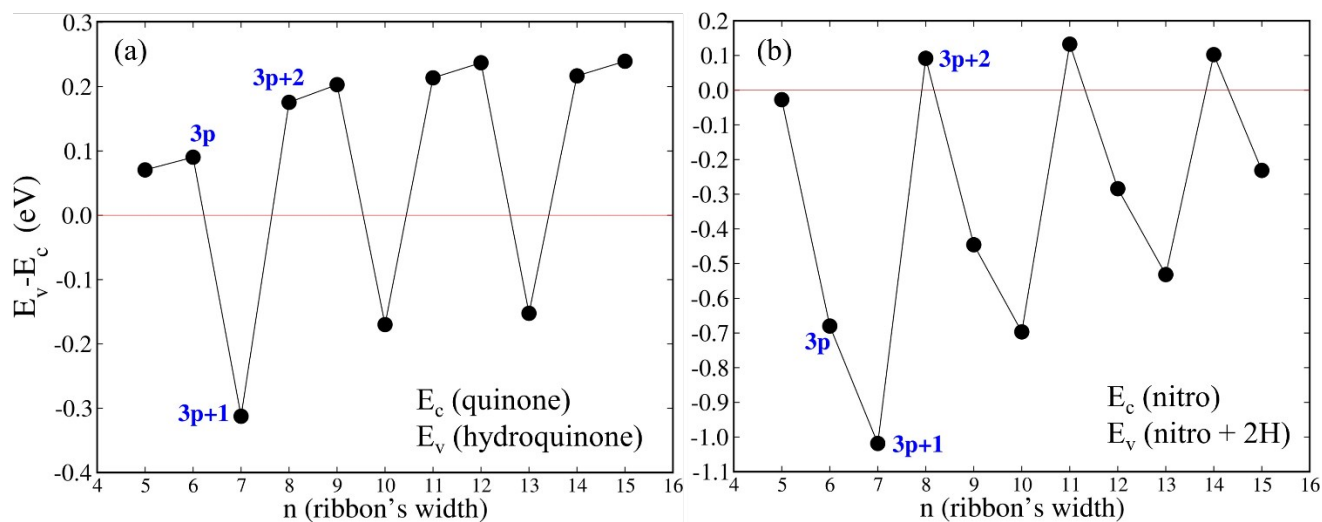
Figure 9: Energy difference between reduction energy and oxidation energy as a function of n (ribbons's width). **(a)** E_c for quinone and E_v for hydroquinone. **(b)** E_c for nitro and E_v for nitro+2H. The corresponding oxidation and reduction energies can be seen in figure 10. The red horizontal line is a guide, showing the zero energy reference.